



Analysis of the local heat transfer of quenching of moving metal sheets made of different materials using flat spray nozzles

Bilal Mehdi¹ · Stephan Ryll¹ · Eckehard Specht¹

Received: 2 February 2023 / Accepted: 21 March 2023 / Published online: 28 April 2023
© The Author(s) 2023

Abstract

Experimental investigations have been performed for the cooling of hot moving metal sheets of thickness 2 mm and 5 mm with the initial temperature of 500 °C to 800 °C by two flat spray nozzles. Tap water at room temperature is used as a coolant. Experiments are carried out for nickel, microfer, and aluminum alloy AA6082 with varying sheet velocity (5, 10, 15 mm/s) and nozzle inclination angle (45°, 65°, 90°). The temperature distribution on the backside of the sheet during the cooling is recorded with a high-speed infrared camera. The recorded thermal data are used in the inverse heat conduction analysis to estimate the local heat fluxes and temperatures on the quenched surface. The thermal images obtained are used to analyze the length of the pre-cooling, transition boiling, and nucleate boiling. The maximum heat flux, the DNB temperature, and the rewetting temperature are presented for researched parameters. The nozzle inclination angle has a weak influence. The higher the velocity and the thickness of the sheet are, the higher the maximum heat flux and the shorter the pre-cooling region. The reason is that the position of the max. heat flux is shifted downstream near to impingement region.

List of notations

3D	Three dimensional
b	Spray width (mm)
B	Impacting length (mm)
CGM	Conjugate gradient method
CHF	Critical heat flux
DNB	Departure nucleate boiling
γ	Conjugate coefficient
H	Distance between nozzle and sheet (mm)
h	Distance between two nozzles (mm)
Hz	Hertz
IR	Infrared recording
J	Gradient of descent
k	Iteration number
M	Total number of measurement points
P	Direction of descent
\dot{q}	Heat flux (MW/m ²)
q_{\max}	Maximum heat flux (MW/m ²)
s	Material thickness (mm)
t	Time (sec)
T	Temperature (°C)
T ₀	Start temperature (°C)

TC	Thermocouple
t_f	Final time (sec)
T _m	Estimated temp- (°C)
T _{rw}	Rewetting temp- (°C)
w _p	Sheet velocity (mm/s)
Y _m	Measured temp- (°C)
z*	Eulerian coordinate (mm)
α	Nozzle inclination angle (degree)
β	Search step size
ε	Stopping criterion
σ	Standard deviation

1 Introduction

The advanced high-strength metallic components found several applications in the automobile, aerospace, and construction industry. Quenching or ultrafast cooling using water is commonly employed during hardening, continuous casting, and thermal treatment of metals. In these processes, the initial metal temperature to be cooled can be up to 1000 °C for steel alloys, or above 500 °C for aluminum alloys. The required surface morphology, microstructure, and mechanical properties of the metal depend on the cooling rate. However, to achieve the aforementioned properties and to reduce inhomogeneities and thermal stresses, the cooling rate or heat transfer must be controlled accordingly. Various cooling

✉ Bilal Mehdi
bilal.mehdi@ovgu.de

¹ Otto-von-Guericke-University Magdeburg, Magdeburg, Germany

techniques are used due to their specific features: pool boiling, jet, spray impingement, and many others. The impinging liquid jets are well known for rapid and extensive heat removal, whereas moderate and uniform cooling sprays are used e.g. during the secondary cooling stage of continuous cooling of steel. The array of water jets from a mold forming a water curtain is used in a direct chill casting process of non-ferrous metals like aluminum, copper, and their alloys. Additionally, the nozzle fields consisting of different nozzle types are utilized, if the being quenched object is dimensionally wide. Heat transfer characteristics are mainly influenced by nozzle parameters, type of metals, sheet velocity, and cooling medium properties and they strongly affect cooling rate and uniformity. Therefore, a comprehensive understanding of these parameters is crucial for the optimization of the cooling system.

The heat released during the quenching process as a function of the surface temperature so-called boiling curve is shown in Fig. 1.

The boiling curve has main characteristic points like the Leidenfrost temperature T_{Le} , the minimum heat flux q_{min} , the maximum heat flux q_{max} , and the departure nucleate boiling temperature T_{DNB} . The partial film boiling and nucleate boiling ranges can be approximated well by a parabolic function which is stated in [1].

Numerous studies have been conducted to determine the heat transfer characteristics such as DNB (departure from nucleate boiling), rewetting temperature, and maximum heat flux during the quenching of metals. Woche et al. [2] investigated DNB (departure nucleate boiling) and rewetting temperatures using the single-flat spray nozzle and a field of full jet nozzles for stationary metal sheets. Waldeck et al. [3] studied the heat transfer in the quenching process with impinging liquid jets and successfully simulated the entire cooling process in the jet quenching process including all

boiling regimes. Gradeck et al. [4] investigated the quenching of a hot rotating cylinder with an initial temperature of 500 °C to 600 °C by a subcooled water jet. The study results showed that cooling rates are greatly affected by the moving velocity of the solid. Vakili and Gadala [5] studied boiling heat transfer on a hot moving plate by a row of multiple impinging water jets and found out that heat transfer in impact zones is influenced by plate velocity. Fujimoto et al. [6] investigated experimentally the heat transfer of a circular water jet on a moving hot steel plate. The researchers reported that heat flux increases and the position of the maximum heat flux shift downstream with an increase in the sheet velocity. Chen et al. [7] studied heat transfer in the case of a circular jet impinging on a moving metal plate and concluded that the overall heat transfer rate is higher in the case of a moving plate than in the stationary one. The jet impingement cooling of a hot moving steel plate at 900 °C initial temperature is investigated by [8]. The research group found that the cooling efficiency increases by increasing the water flow rate, nozzle height, and the speed of the plate up to a maximum value and then decreases.

Conventionally, the embedded thermocouples are used to measure the temperature profiles, which limits the spatial resolution because the thermocouples cannot be physically installed as close as possible to the quenched surface. This impediment poses a challenge to accurate measurement of temperatures, where the temperature drops rapidly due to high-temperature gradients. For that reason, the University of Magdeburg has been focusing on the contactless measurement infrared thermography technique, which can be found in several dissertations [9–11]. It has been employed in scientific research [12–14] since 2003, which is a very effective technique for temperature measurements. Labergue et al. [15] used an infrared camera for temperature measurements during the cooling of a hot surface using sprays and jets.

In the literature, many studies can be found in the field of cooling hot moving and stationary metal plates to study heat transfer using water jets but relatively fewer scientific investigations are available for flat spray quenching of metals. Henceforth, the current research is focused on the cooling of moving metal sheets using a combination of two flat spray nozzles. The final goal of this research is to find the influence of various parameters, i.e. nozzle inclination angle, metal type, sheet thickness, and sheet velocity, on the local heat transfer and maximum heat flux. The local heat flux on the quenched side is determined using a two-dimensional inverse heat conduction problem. The temperature field on the rear face (opposite side of the impingement) is measured by infrared thermography. Additionally, a 3D-numerical model for moving sheets based on the Eulerian approach is developed at Bremen University. The conjugate heat transfer problem is solved in two-phase numerical modeling in commercial software ANSYS Fluent, in which water acts

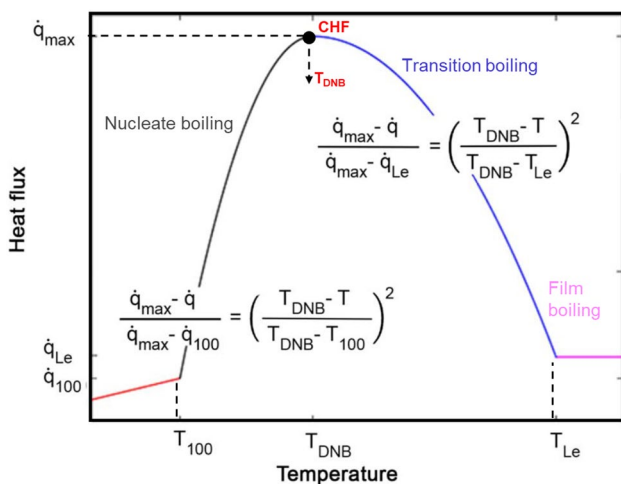


Fig. 1 Parabolic approximation of the boiling curve

as a continuous phase and vapor as a dispersed phase. The model is validated with the experimental data and can successfully simulate all quenching regions during cooling. Further details about the model can be found in [16–18].

2 Measuring and analysis method

2.1 Experimental facility

In the experiments, vertically moving hot metal sheets are quenched from high temperatures by two flat sprays. The experimental setup is illustrated in Fig. 2.

The sheet is electrically heated to the desired starting temperature in a furnace and then transferred to the cooling chamber using sliding rails, where it is positioned in front of the nozzles. The sheet is moved vertically using a traverse and is quenched by flat sprays under controlled conditions. Meanwhile, the temperature of the sheet that is being cooled is recorded from the back side with a high-speed infrared camera of 200 fps frame rate. The measurement range for the camera is 150 °C to 1000 °C.

Aluminum alloy (AA6082), nickel, and nicrofer sheets (250 × 230 mm) of 2 mm and 5 mm thickness were heated in the furnace up to a homogenous start temperature in the range of 500 to 800 °C. The sheet velocities are varied from 5 to 15 mm/s. The rear side of the metal sheet is coated with black paint of high (approximately 0.93) temperature-stable emissivity necessary for accurate infrared recordings.

A calibration experiment has been performed for the validation of IR camera measurements. A thermocouple (TC) is installed 1 mm below the surface of a 10 mm stainless steel plate and the temperature profiles are compared with surface temperature recordings of the IR camera. The sheet temperature was held and at constant a temperature, the deviance between both measurements is ± 1 K. During the plate cooling in the air with a start temperature of 850 °C,

a temperature difference of 11 K was observed between TC and IR camera measurements due to the depth of the TC. The emissivity of the used black coating was determined to be 0.93 ± 0.02 independent of temperature.

The flat spray is characterized by spray angle (β), spray width (b), and impacting length (B) that then forms a rectangular shape liquid film on the hot surface, as shown in Fig. 3. The spray nozzle field of two flat sprays 35 mm apart from each other is used for experimental investigations. The water pressure was kept at 2 bar constant and the temperature was set to 22 °C.

A distance of 50 mm was maintained between the nozzles and the sheet. To avoid start-up irregularities, a protection sheet or splash shield was used and removed before the quenching process started, so that fully formed water jets hit the hot sheet.

Figure 4 shows a camera snapshot of a flat spray impinging on a hot surface.

It can be seen that the area close to the stagnation point is wetted and the rectangular-shaped wetting front propagates outward. Due to the liquid evaporation process, the liquid film disrupts the surface and forms droplets. These droplets fly outwards, leaving the surface behind dry, and consequently, without any cooling effect on the surface. Transition and nucleate boiling occur in this region.

2.2 Impingement flux

For flat sprays, the volume flow rate is used as a characteristic parameter. The total volume flow rate of the water that impinges on the surface with a width of 80 mm is equal to 25 L/min m. The impingement flux and its local distribution is another important influencing factor for flat sprays and is measured using a patternator, which is built and designed in our lab by our lab technicians. Figure 5 shows the patternator schematics and the profile of impingement flux for two flat sprays at a constant pressure of 2 bar. The impingement

Fig. 2 Schematic diagram of the experimental set-up

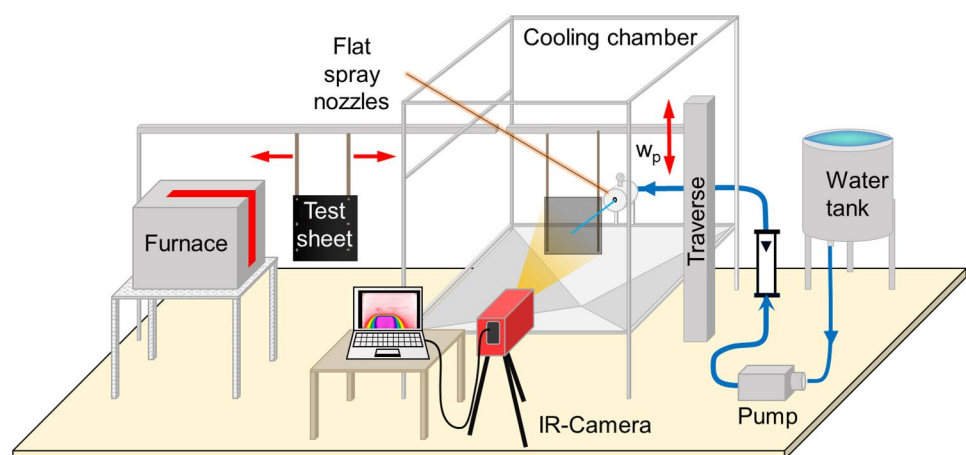
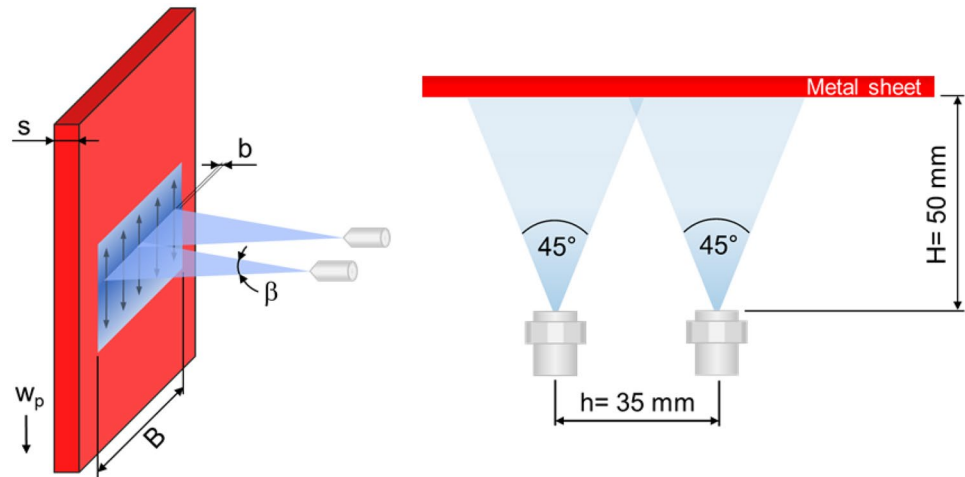


Fig. 3 Schematic representation of two flat sprays



setup consists of nozzles 35 mm apart nozzles facing downwards mounted on a stand. The stand can be precisely controlled and moved in all three dimensions with an accuracy of millimeters. Below the nozzles, there is a board having 10 mm small cylindrical tubes of 10 mm diameter arranged in a linear array, which are further connected with small water collecting bottles.

The maximum spray flux is obtained in the middle of the two sprays, due to the superposition. It can be seen that between the -10 and 10 mm range, the impingement flux is maximum and does not change significantly. For that reason, the measuring line is drawn along the center of the two sprays during the processing of experimental data.

2.3 Infrared recording

In the present study, an infrared camera ‘ImageIR 8800’ from ‘InfraTec GmbH’ is used with a frequency of 200 Hz and a resolution of 640×512 pixels. An infrared image of a 5 mm thick nickel sheet is illustrated in Fig. 6. The sheet is moving with 5 mm/s velocity and its corresponding profile at the time instant 10 s can be seen. For the extraction of

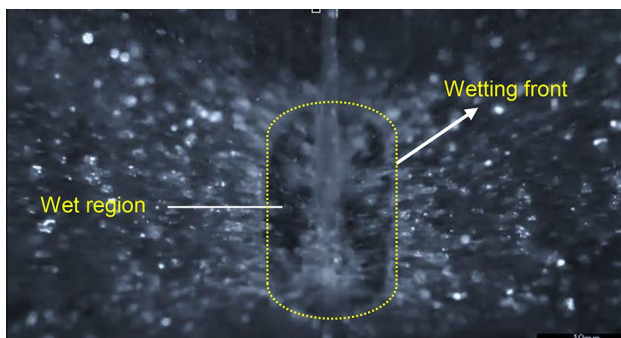


Fig. 4 A high-speed camera image of impinging a single flat spray on the hot sheet

temperatures during the cooling process, measuring lines L1, L2, and L3 are drawn.

The top side of the sheet has a high temperature close to the start temperature of 800 °C and it decreases sharply as the wetting front or wetted region approaches. Temperature profiles for these measuring lines show a uniform homogeneous cooling and all three profiles are quite the same, due to the propagation of the rectangular wetting front.

For analysis, the measuring line is drawn for all experiments in the middle of two interacting nozzles, where the maximum spray flux and consequently, the highest heat flux occurs.

2.4 Boiling regions

As the water from the nozzle hits the hot moving sheet, three regions form on it. The schematic representation of these regions (A, B, C) and the corresponding temperature profile can be seen in Fig. 7.

The temperatures are plotted against the sheet length, where $z^* = 0$ shows the position of the nozzle or impingement point on the sheet. The negative range of z^* shows

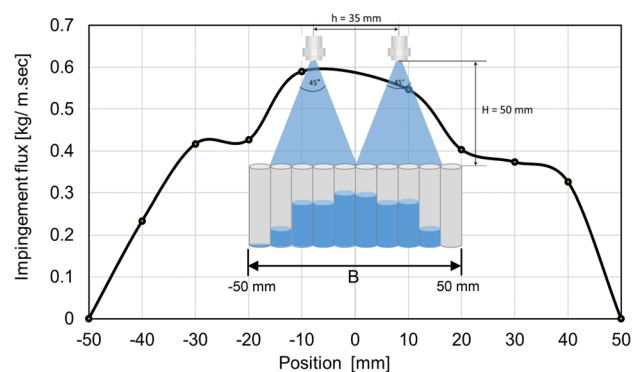
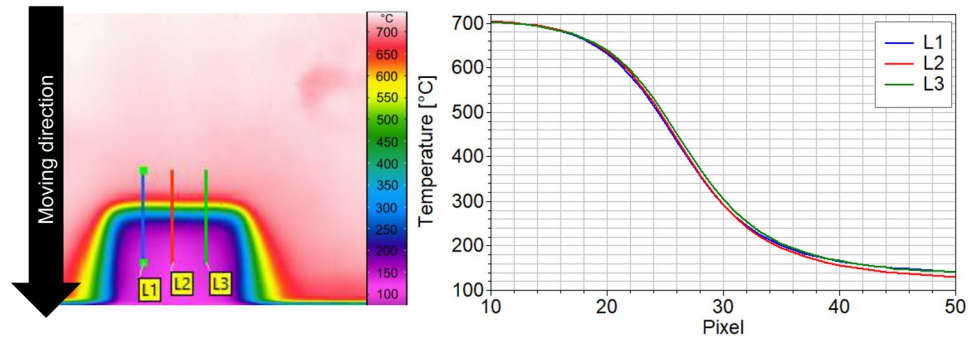


Fig. 5 Impingement flux along the spray axis

Fig. 6 An infrared image and corresponding cooling curve

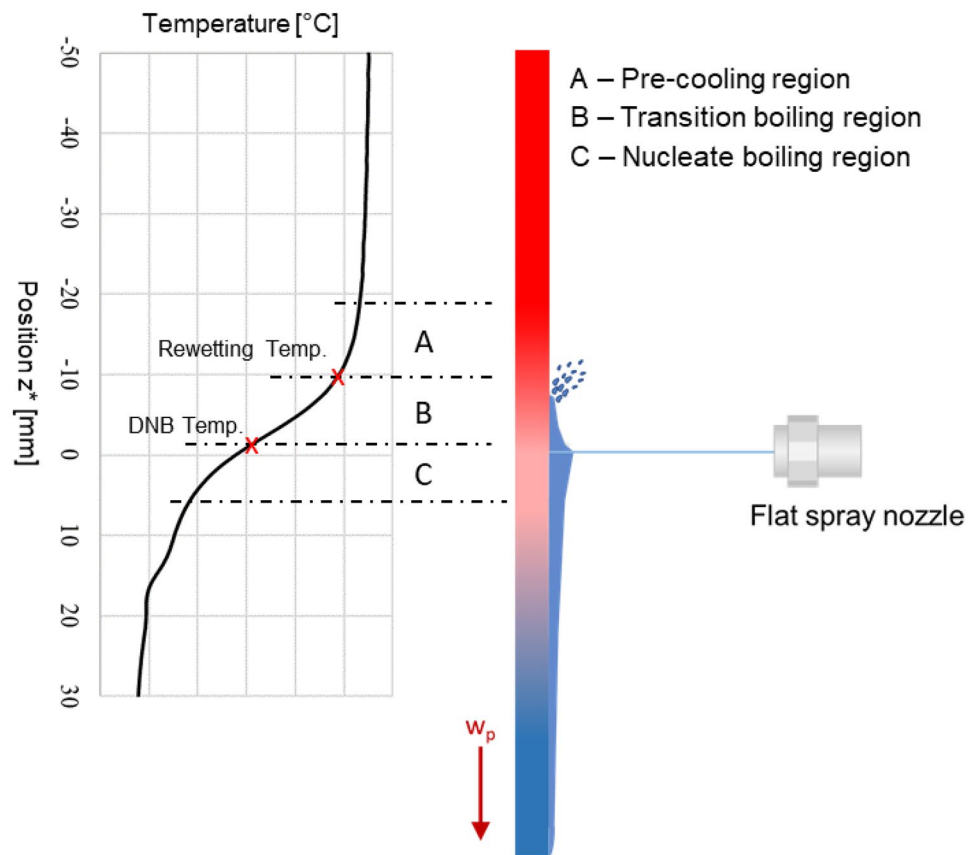


the top hot part of the sheet. The temperature starts decreasing before the wetting front approaches, it is due to axial heat conduction and is known as the pre-cooling region. In metals with high thermal conductivity, such as Aluminium, the temperature drops more sharply in this region. The rewetting temperature is the temperature at which the sheet is wet by water and starts cooling down due to water quenching. The region between the rewetting temperature T_{rw} and the DNB (departure from nucleate boiling) is the transition boiling region. The nucleate boiling region starts after DNB where the maximum heat flux q_{max} is obtained.

2.5 Inverse heat conduction method

For the heat transfer analysis, the temperatures of the quenched surface are required. Therefore, these temperatures have to be calculated using the measured surface temperatures on the back side of the sheet. For this calculation, an inverse heat conduction method was applied. Inverse modeling has caught real attention due to its unique applications in recent years and many inverse models have been developed by several researchers to determine heat flux or heat transfer coefficient. A one-dimensional heat conduction formulation based on a sequential function specification

Fig. 7 Different regions and temperature profile along the sheet length during the cooling



method has been developed by B. Wang et al. [19] to estimate heat flux during jet impingement on a high-temperature plate surface. Nallathambi and Specht [20] used the two-dimensional finite element method to estimate the heat flux during the metal quenching process using an array of jets. Z. Malinowski et al. [21] developed an inverse method to determine three-dimensional heat flux and heat transfer coefficient distributions in space and time over a metal surface cooled by water.

In the present study, the inverse heat transfer problem is solved using a conjugate gradient method with an adjoint problem; more details about this method can be found in M. Özisik [22].

The method minimizes the objective function, which is given by Eq. (1)

$$J[\dot{q}(y, t)] = \sum_{t=0}^{t_f} \sum_{m=1}^M (T_m(t) - Y_m(t))^2 \tag{1}$$

The objective function involves the squared difference between the measured temperature $Y_m(t)$ with the help of the infrared camera and the calculated temperatures $T_m(t)$ estimated with the direct problem by using the estimated heat flux $\dot{q}(y, t)$ on the quench side, t_f represents the final time, and M is the total number of measurement points on the quench surface (number of pixels).

The CGM (conjugate gradient method) is an iterative method that converges to a minimum of the objective function. At each iteration the estimated heat flux $\dot{q}(y, t)$ is computed using Eq. (2)

$$\dot{q}^{k+1}(y, t) = \dot{q}^k(y, t) - \beta^k P^k(y, t), \tag{2}$$

where β^k is the search step size, P^k the direction of descent and k the iteration number.

The direction of descent is a linear combination of the gradient direction with the previous iteration’s direction of descent, which is given below in Eq. (3)

$$P^k(y, t) = J^k(y, t) + \gamma^k P^{k-1}(y, t). \tag{3}$$

The conjugate coefficient γ can be calculated using Eq. (4) as done in [22]

$$\gamma^k = \frac{\sum_{t=0}^{t_f} \sum_{m=1}^M (J^k)^2}{\sum_{t=0}^{t_f} \sum_{m=1}^M (J^{k-1})^2}. \tag{4}$$

The stopping criterion is given by

$$\varepsilon = M\sigma^2 t_f, \tag{5}$$

$$\sigma = T_m(t) - Y_m(t), \tag{6}$$

where σ is the standard deviation of the temperature measurements and is assumed to be constant.

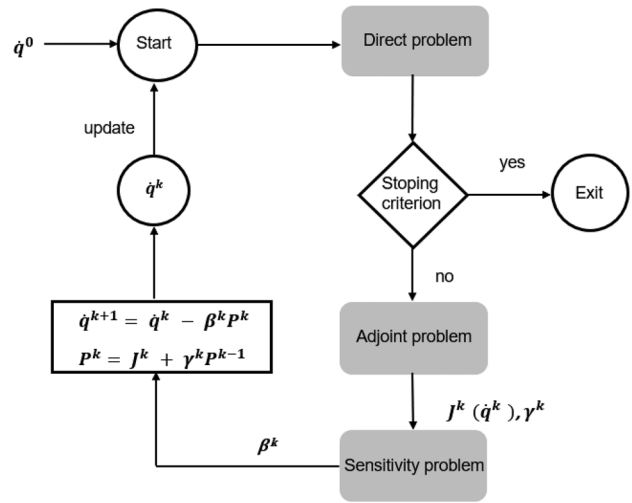


Fig. 8 Flowchart for the inverse method algorithm

To perform the iterative process, first the step size β and the gradient of descent $J^k(y, t)$ are computed by solving the sensitivity and adjoint problems [22]. As stated in [22] these problems can be transformed into a simple Fourier law problem by specifying boundary and initial conditions. These problems are solved numerically using the finite difference method. For further details of these problems, the reader is referred to [23–25].

Figure 8 shows, a simplified flowchart for the inverse heat conduction solution algorithm.

- Step 1. Solve the direct problem ($T(x, y, t)$) using the initial guess of the boundary condition $q^0(y, t)$
- Step 2. Check the stopping criterion given by Eq. (5). Continue if not satisfied
- Step 3. Compute the gradient direction $J^k(y, t)$ from the adjoint problem and then the conjugate coefficient γ^k from Eq. (4).
- Step 4. Compute the direction of descent P^k using Eq. (3).

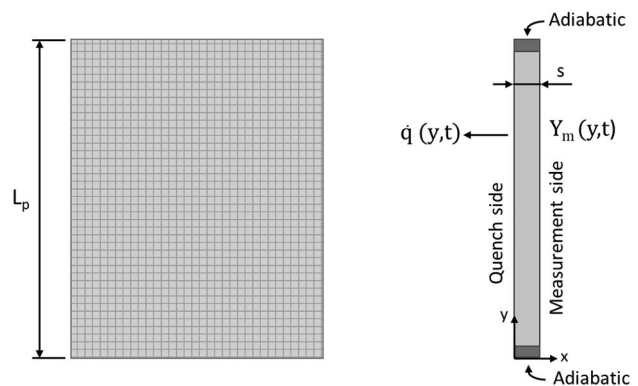


Fig. 9 Schematic representation of the sheet

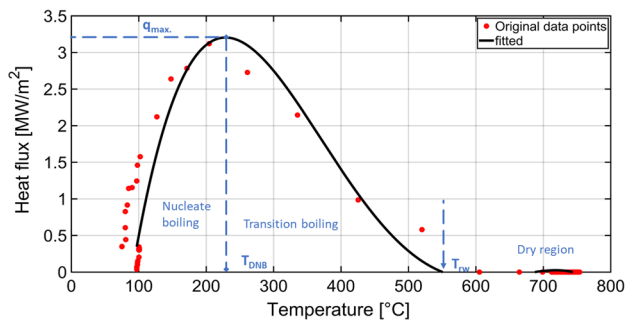


Fig. 10 Smoothed Heat flux vs Temperature on the quenched side

Step 5. Compute the new search step size β^k solving the sensitivity problem.

Step 6. Compute the new estimation for \dot{q}^{k+1} and return to step 1.

To evaluate the heat flux, the iterative method described above is applied to the 2D structure, as shown in Fig. 9.

Apart from the quenched surface, all other thermal boundaries are assumed as adiabatic to simplify the problem and no cooling in the width direction is assumed. The measured spatial and temporal temperature ($Y_m(y, t)$) along the y -axis from the measurement side is used to numerically solve the problem in the y and x directions to obtain heat flux along the y -axis on the quenching side. MATLAB R2021a software is used for numerical and inverse calculations.

The surface heat flux approximated through the inverse heat transfer method is plotted in Fig. 10 as a function of the quenched surface temperature for a 2 mm nickel sheet as an example, this profile is called the boiling curve.

The red colored points show the original data points obtained from the inverse solution. As the inverse heat transfer methods give very unstable fluctuating results, it requires fine smoothing and fitting of results. The black curve shows the best fitting of the original solution, the data points are fitted using the polynomial function of order 4. The data is fitted using the OriginPro 2021 software, the statistics of the fitting are shown in Table 1. This technique is employed so that the effect of various parameters on heat flux can be better understood. The curve is divided into three regimes: dry region, transition boiling region, and nucleate boiling region. The cooling starts when the rewetting temperature T_{rw} of 560 °C is reached and heat flux starts rising. The

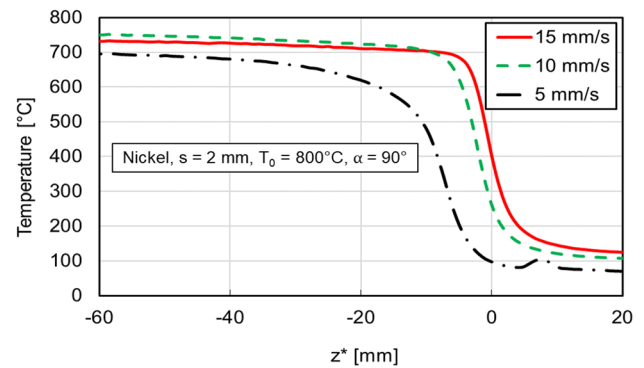


Fig. 11 Cooling curves for various sheet velocities with a nozzle angle of 90°

transition boiling region is in a range from 560 °C to 220 °C. The maximum value of 3.3 MW/m² of heat flux occurs at $T_{DNB} = 220$ °C. Nucleate boiling follows the transition boiling, in which the evaporation rate and the heat flux decrease due to the low surface temperature and small bubble nuclei formation on the surface.

3 Results and discussions

In the following, the fitted boiling curves are compared for nickel, microfer, and aluminum alloy (AA6082) to determine the influence of parameters such as sheet thickness s , the nozzle angle α , and the sheet velocity w_p .

3.1 Nickel

The temperature profiles of 2 mm nickel sheets with a nozzle angle of 90° for different sheet velocities are depicted in Fig. 11.

The cooling curves along the sheet length are chosen after some time at the so-called quasi-stationary time, to avoid start-up disruptions. On the left side (negative z^*) the sheet has the initial temperature before quenching and on the right side (positive z^*) the sheet is cooled by the spray. The zero on the x -axis shows the position of the spray impact on the sheet. The red curve shows the decrease in temperature for a maximum sheet velocity of 15 mm/s and the black represents the minimum sheet velocity of 5 mm/s. It can be seen, that all temperature curves start to drop before the impingement point. The reason is the axial heat conduction and the

Table 1 Statistics of fitting

Number of points	Degrees of freedom	Reduced chi-square	Residual sum of squares	R-square (COD)	Adj. R-square	Fit status
193	183	0.0567	10.37	0.85	0.84	succeeded

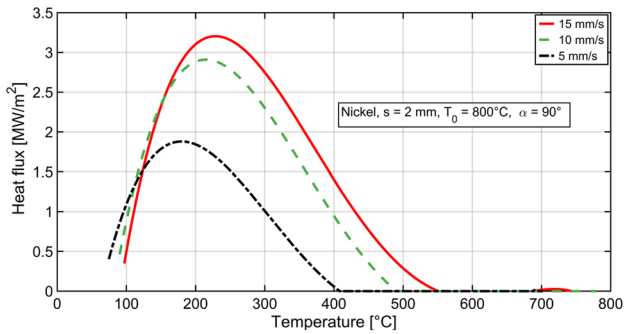


Fig. 12 Heat flux curves for different sheet velocities

movement of the wetting front in the upward direction. As the sheet velocity w_p increases from 5 to 15 mm/s, the temperature in the vicinity of the impingement region increases from 100 °C to 400 °C, and as a result, the pre-cooling effect reduces.

The heat flux curves estimated from the cooling curves for varying sheet velocities are illustrated in Fig. 12. The heat flux in total as well as the maximum heat flux are higher with increasing sheet velocity. The DNB temperatures are in the range of 180 °C to 220 °C and the rewetting temperature increases from 400 °C to 550 °C. The higher sheet velocities cause a minor increase in DNB temperature.

Similarly, the cooling profiles at a nozzle angle of 65° for 2 mm nickel with varying sheet velocity w_p are shown in Fig. 13. There is no significant influence of the nozzle angle on the cooling curve rather than the increase in temperature at the impingement point ($z^* = 0$).

The corresponding heat flux curves for the nozzle angle of 65° can be seen in Fig. 14.

Figure 15 shows the comparison of the maximum heat fluxes of the three investigated nozzle angles for 5, 10 and 15 mm/s sheet velocities.

The highest maximum heat flux q_{max} is obtained for the 65° angle shown by the yellow curve. There is no substantial change of heat flux for 90° and 45° angles.

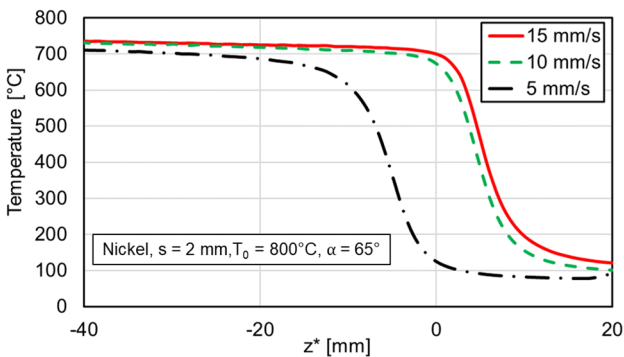


Fig. 13 Cooling curves for various sheet velocities with nozzle angle 65°

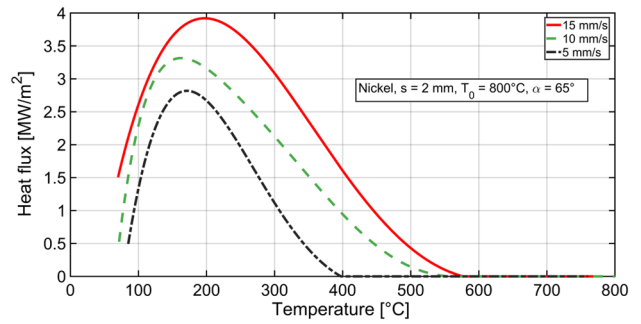


Fig. 14 Heat flux curves for different sheet velocities

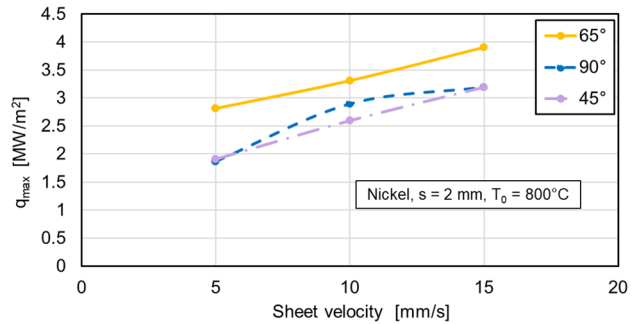


Fig. 15 Influence of inclination angle on the max. heat flux

The influence of varying angles on the local position of T_{DNB} is shown in Fig. 16. The z^* at 0 mm shows the impingement point at the sheet from the nozzles, the negative range ($z^* < 0$) shows the upstream, and the positive range ($z^* > 0$) represents the downstream region. It can be seen that the DNB temperature for all inclination angles increases with increasing sheet velocity. Generally, the DNB temperatures are higher at 90° and lower at 65° inclination angle.

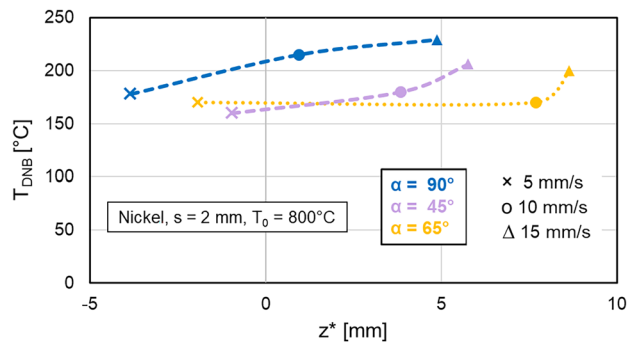


Fig. 16 T_{DNB} vs the local position at various nozzle angles

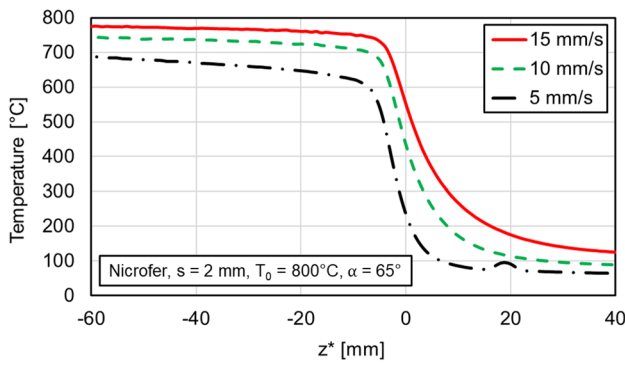


Fig. 17 Cooling curves for various sheet velocities with nozzle angle 65

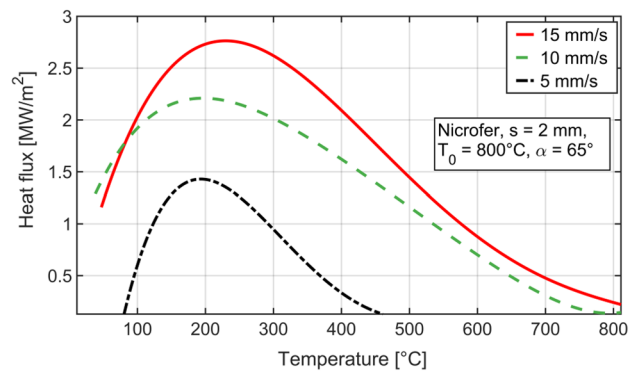


Fig. 18 Heat flux curves for different sheet velocities

3.2 Nicrofer

In this section, the heat transfer for nicrofer as a material is discussed. Figure 17 shows the temperature profiles during the cooling for various sheet velocities at a nozzle angle of 65°.

In comparison to Fig. 13 for nickel, it can be seen that the temperature at the impingement point ($z^* = 0$) for 5 mm/s sheet velocity is about 100 °C higher. The reason is the shorter pre-cooling region because of the lower thermal conductivity. Table 2 summarises the thermo-physical material properties of the three metals at the ambient temperature used in the present study. Nicrofer has a three times lower thermal conductivity than nickel.

For all three velocities, the sheets cool down at quasi-stationary conditions. The temperatures are 230 °C, 440 °C, and 580 °C at the impingement point for 5 mm/s, 10 mm/s, and 15 mm/s moving sheets, respectively. By increasing the moving velocities, the rate of cooling increases. Due to the lower thermal conductivity of nicrofer, it cools down slower compared to nickel.

Figure 18 shows the boiling curves for nicrofer with varying sheet velocities. The higher the sheet velocity is the higher is again the maximum heat flux, the rewetting temperature, and the DNB temperature. Compare to nickel, the maximum heat flux for nicrofer is lower whereas the DNB temperature is higher.

Figure 19 shows the maximum heat flux dependent on the sheet velocity for the two nozzle angles of 65° and 45°.

Table 2 Material properties of investigated Metals

Metal	Thermal conductivity (W/m.K)	Density (Kg/m ³)	Specific heat capacity (J/Kg.K)
Nickel	70	8900	500
Nicrofer	20	8400	510
AA6082	170	2700	1050

The maximum heat flux is a little higher in the case of 65° angle than 45°. The influence however is again relatively low.

3.3 AA6082

The temperature profiles for the cooling of the aluminum alloy (AA6082) sheets are shown in Fig. 20.

It can be seen, that AA6082 sheets are already cooled when they reach the impingement position at $z^* = 0$. The reason is the very high thermal conductivity which results in a large pre-cooling range.

In Fig. 21 the heat flux profiles versus the surface temperatures are depicted.

The maximum heat flux for AA6082 is comparatively lower than the other two materials (nickel, and nicrofer). The DNB and the rewetting temperatures are also comparatively lower. The reason is the lower initial temperature because of the low melting point, it can not be heated to 800 °C.

Figure 22 shows the influence of the nozzle angle. The influence is again very low, however, at the nozzle angle of 65°, the heat flux is maximum.

Figure 23 shows the cooling profiles of AA6082 sheets with a thickness of 5 mm instead of 2 mm. For 5 mm

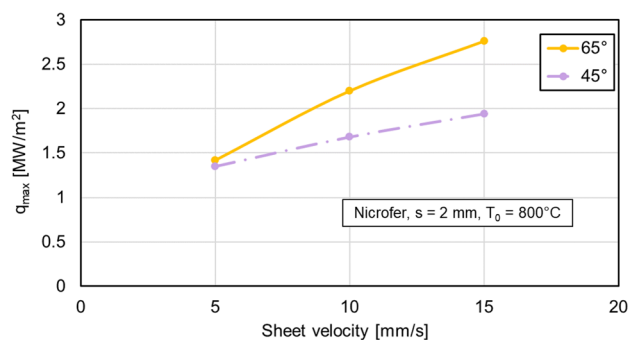


Fig. 19 Angle comparison for maximum heat flux and sheet velocity

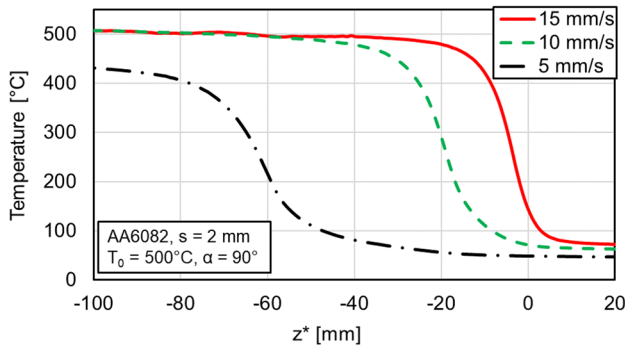


Fig. 20 Cooling curves for different sheet velocities at nozzle angle 90°

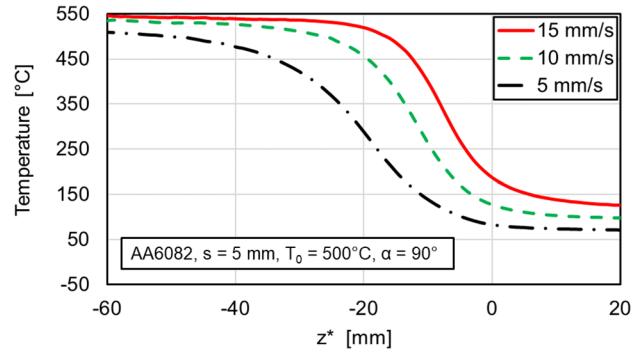


Fig. 23 Cooling curves for different sheet velocities for a 5 mm thick AA6082 sheet

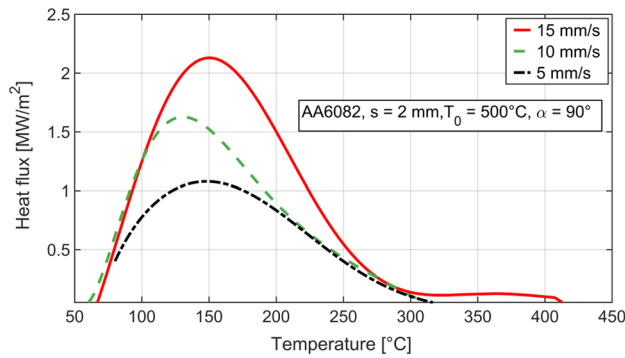


Fig. 21 Heat flux curves for different sheet velocities

thickness, the pre-cooling range is much shorter which results in a higher temperature at the impingement point.

Figure 24 shows the corresponding heat fluxes for a 5 mm AA6082 sheet at 5, 10, and 15 mm/s sheet velocities.

The maximum heat fluxes are significantly higher as compared to the 2 mm AA6082 sheet at the same sheet velocities.

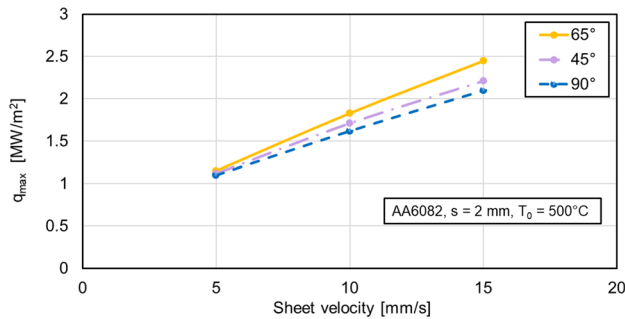


Fig. 22 The maximum heat flux vs sheet velocities for various nozzle angles

3.4 Mechanism of heat transfer

The mechanism of heat transfer is influenced by the water flow rate and type of metal. As the water flow rate is much higher than the sheet velocity, it must be independent of the sheet velocity as well as the sheet thickness. Therefore, the heat transfer is dependent on the local position (z^*) on the sheet. It is higher near the impingement point and decreases away from the impact point. It can be seen in all-temperature profiles, that the DNB temperature with the maximum heat flux is obtained always in the downstream zone below the impingement point ($z^* > 0$). The higher the sheet velocity becomes the more the DNB temperature is shifted near the impingement region which results in a higher value of the maximum heat flux. A similar effect is valid for increasing sheet thickness. As the sheet thickness increases, the DNB temperature is shifted near to impingement region which causes the maximum heat flux. Therefore, in the following figures, the maximum heat flux is shown against the local position (z^*).

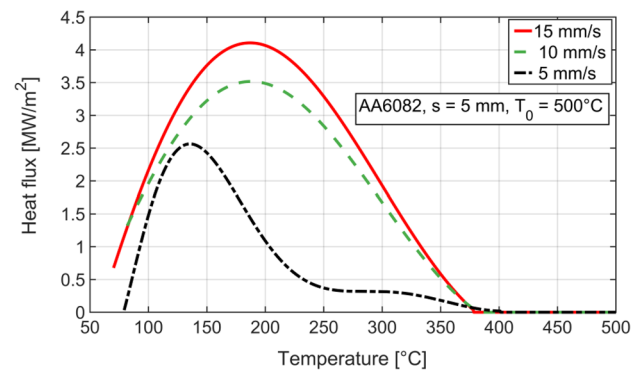


Fig. 24 Heat flux curves for different sheet velocities for a 5 mm thick AA6082 sheet

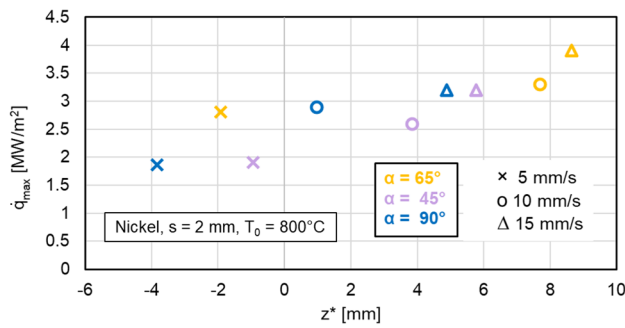


Fig. 25 Maximum heat flux vs local position z^* at various nozzle angles

The nozzle inclination angle influences the propagation of the wetting front in the upstream and the downstream zones, which further changes the width of the pre-cooling and quenching regions. Hence, the maximum heat flux varies with it. Figure 25 shows the influence of nozzle angle for nickel on maximum heat flux at various sheet velocities.

It can be seen that for all nozzle inclination angles, the maximum heat flux increases with increasing sheet velocity, and the local position of the maximum heat flux shifts to the downstream zone below the impingement point ($z^* > 0$).

In Fig. 7 various regions are displayed on the cooling curve. As the infrared camera allows the full view of temperature data, the width of these boiling regions can be measured visually. Table 3 shows the widths of various boiling regions for the 2 mm nickel sheet at various velocities.

The front width in the pre-cooling region decreases with an increase in sheet velocities, at 5 mm/s it is 16 mm, and at 15 mm/s is 4 mm. However, the width of the nucleate boiling regions increases with the increase in sheet velocity.

Similarly, in Fig. 26 the maximum heat flux for microfer against z^* at various nozzle inclination angles and sheet velocities is shown. Microfer follows a similar trend as nickel that maximum heat flux shifts downstream at higher velocities for both angles.

Table 4 depicts the width of different cooling regions for microfer at a nozzle inclination angle of 65°.

The width of the pre-cooling region is 1 mm shorter at higher velocities, whereas the width of transition and nucleate boiling regions increases with increasing velocities.

Table 3 Width of various quenching regions for a nickel at various sheet velocities

Sheet velocity	5 mm/s	10 mm/s	15 mm/s
Pre-cooling region	9 mm	4 mm	3 mm
Transition boiling region	6 mm	4 mm	4 mm
Nucleate boiling region	5 mm	10 mm	32 mm
Rewetting Temp- (T_{rw})	400 °C	500 °C	550 °C
DNB Temp- (T_{DNB})	190 °C	210 °C	220 °C

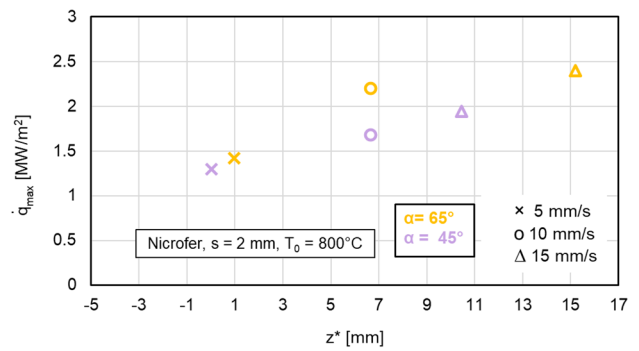


Fig. 26 Maximum heat flux vs local position z^* at various nozzle angles

Table 4 Width of various quenching regions for a microfer at various sheet velocities

Sheet velocity	5 mm/s	10 mm/s	15 mm/s
Pre-cooling region	5 mm	4 mm	4 mm
Transition boiling region	6 mm	9 mm	14 mm
Nucleate boiling region	5 mm	9 mm	28 mm
Rewetting Temp- (T_{rw})	480 °C	780 °C	800 °C
DNB Temp- (T_{DNB})	200 °C	200 °C	220 °C

For 2 mm AA6082, Fig. 27 presents the maximum heat flux vs local position z^* at various sheet velocities and nozzle inclination angles. Due to the high thermal conductivity of AA6082, the maximum heat flux for all velocities is obtained in the upstream region. Although, the position of max. heat flux shifts near to impingement point at higher velocities.

Table 5 shows the front widths of various regions during the cooling of 2 mm AA6082 at a 90° nozzle angle.

The front widths of all the quenching regions decrease with increasing sheet velocities.

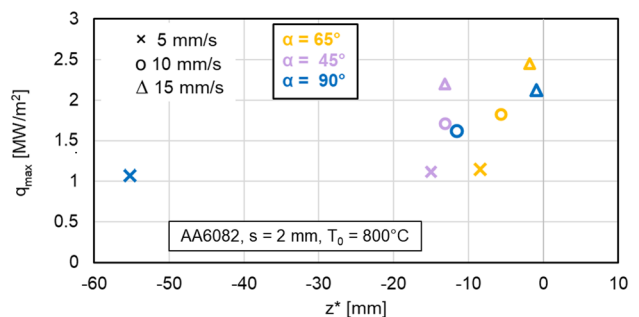


Fig. 27 Maximum heat flux vs local position z^* at various nozzle angles

Table 5 Width of various quenching regions for AA6082 at various sheet velocities

Sheet velocity	5 mm/s	10 mm/s	15 mm/s
Pre-cooling region	15 mm	9 mm	6 mm
Transition boiling region	9 mm	9 mm	6 mm
Nucleate boiling region	7 mm	5 mm	4 mm
Rewetting Temp- (T_{rw})	330 °C	332 °C	335 °C
DNB Temp- (T_{DNB})	150 °C	145 °C	150 °C

4 Conclusion

The results of the current study indicate that the cooling of hot sheets by flat sprays is influenced by several parameters such as sheet velocity, sheet thickness, material type, and nozzle inclination angle. Based on the findings, the following can be concluded:

By varying the sheet velocity, it is observed that increasing the sheet velocity results in an increase in the maximum heat flux, while the front width of the pre-cooling region decreases. As the sheet velocity increases, the water spray impinges on the surface, which has a higher temperature because of the low axial pre-cooling effect. Therefore, the highest heat transfer and cooling occur in the vicinity of the impingement region, resulting in the highest heat flux in that area. The results show that sheet velocity is a vital parameter and a suitable sheet velocity must be selected considering maximum heat flux to achieve homogenous cooling. The DNB temperature increases along with it as well, but not significantly as the maximum heat flux.

The variation of sheet thickness shows the same trend as the sheet velocity, the maximum heat flux increases for thicker sheets, due to a decrease in the front width of pre-cooling. This means that the pre-cooling process, which involves cooling the sheet before it enters an impingement region has a smaller effect on the thicker sheet compared to a thinner sheet. As a result, the front width of pre-cooling decreases for thicker sheets, which leads to an increase in the maximum heat flux.

The pre-cooling effect in the axial direction for the Aluminum alloy AA6082 (highly conductive metal) and thin plates of 2 mm thickness is higher and therefore the width of the pre-cooling region is larger. This effect causes a drop in maximum heat flux

Furthermore, by varying the nozzle inclination angle, it is observed that the nozzle angle has a minimum influence during the cooling, and for the 65° inclination angle q_{max} is comparatively higher. More research is needed to better understand the influence of nozzle angle on thicker plates.

The infrared images are used to observe the width of various cooling regions and observed that for all three investigated metals, the length of the pre-cooling region decreases by increasing sheet velocities, and sheet thickness, in result maximum heat flux increases. The local position of DNB temperature shifts towards the impingement region with an increasing sheet velocity. The DNB temperatures for Nickel and Nicrofer are between 190 °C and 220 °C and for AA6082 from 140 °C to 160 °C.

Author contributions All authors contributed to the study conception and design. Material preparation, data collection and analysis were performed by [Bilal Mehdi], [Stephan Ryll] and [Eckehard Specht]. The first draft of the manuscript was written by [Bilal Mehdi] and all authors commented on previous versions of the manuscript. All authors read and approved the final manuscript.

Funding Open Access funding enabled and organized by Projekt DEAL. The project is financially funded by the German Federal Ministry for Economic Affairs and Climate protection through the Industrial Research Association “Otto von Guericke” (AiF) and promoted by the Research Foundation “Industrial Furnaces”.

Data availability Data can be made available on request.

Declarations

Competing interests The authors have no relevant financial or non-financial interests to disclose.

Open Access This article is licensed under a Creative Commons Attribution 4.0 International License, which permits use, sharing, adaptation, distribution and reproduction in any medium or format, as long as you give appropriate credit to the original author(s) and the source, provide a link to the Creative Commons licence, and indicate if changes were made. The images or other third party material in this article are included in the article's Creative Commons licence, unless indicated otherwise in a credit line to the material. If material is not included in the article's Creative Commons licence and your intended use is not permitted by statutory regulation or exceeds the permitted use, you will need to obtain permission directly from the copyright holder. To view a copy of this licence, visit <http://creativecommons.org/licenses/by/4.0/>.

References

1. Specht E (2018) Heat and mass transfer in thermal process engineering. Vulkan Verlag (Essen, Germany), pp 241–242
2. Woche H, Fang Y, Specht E (2018) Heat transfer analysis during metal cooling with sprays and jets. Heat processing (magazine). Vulkan-Verlag 01/2018:41–47
3. Waldeck S, Woche H, Specht E, Fritsching U (2018) Evaluation of heat transfer in quenching processes with impinging liquid jets. Int J Therm Sci 134:160–167
4. Gradeck M, Kouachi A, Borean J-L, Gardin P, Lebouché M (2011) Heat transfer from a hot moving cylinder impinged by a planar subcooled water jet. Int J Heat Mass Transf 54:5527–5539
5. Vakili S, Gadala MS (2013) Boiling Heat Transfer of Multiple Impinging Jets on a Hot Moving Plate. Heat Transfer Eng 34(7):580–595

6. Fujimoto H, Tatebe K, Shiramasa Y, Hama T, Takuda H (2014) Heat Transfer Characteristics of a Circular Water Jet Impinging on a Moving Hot Solid. *ISIJ Int* 54(6):1338–1345
 7. Chen S, Kothari J, Tseng A (1991) Cooling of a moving plate with an impinging circular water jet. *Exp Thermal Fluid Sci* 4(3):343–353
 8. Jha J, Ravikumar SV, Sarkar I, Pal SK, Chakraborty S (2016) Jet Impingement Cooling of a Hot Moving Steel Plate: An Experimental Study. *Exp Heat Transf* 29(5):615–631
 9. Fang Y (2019) Influence of nozzle type and configuration and surface roughness on heat transfer during metal quenching with water. Otto-von-Guericke University Magdeburg, Dissertation
 10. Attalla M (2005) Experimental Investigation of Heat Transfer Characteristics from Arrays of Free Impinging Circular Jets and Hole Channels. Otto-von-Guericke University Magdeburg, Dissertation
 11. Puschmann F (2003) Experimentelle Untersuchung der Spraykühlung zur Qualitätsverbesserung durch definierte Einstellung des Wärmeübergangs. Otto-von-Guericke-Universität Magdeburg, Dissertation
 12. Vintrou S, Bougeard D, Russeil S, Nacereddine R, Harion J (2013) Quantitative infrared investigation of local heat transfer in a circular finned tube heat exchanger assembly. *Int J Heat Fluid Flow* 44:197–207
 13. Bougeard D (2007) Infrared thermography investigation of local heat transfer in a plate fin and two-tube rows assembly. *Int J Heat Fluid Flow* 28(5):988–1002
 14. Fénot M, Vullierme J, Dorignac E (2005) A heat transfer measurement of jet impingement with high injection temperature. *Comptes Rendus Mécanique* 333(10):778–782
 15. Labergue A, Gradeck M, Lemoine F (2015) Comparative study of the cooling of a hot temperature surface using sprays and liquid jets. *Int J Heat Mass Transf* 81:889–900
 16. Narayan NM, Fritsching U, Mehdi B, Gopalkrishna SB, Woche H, Specht E (2021) Investigation of heat transfer in arrays of water jets modelling/simulation and experimental approach. In the ECHT-European Conference on Heat Treatment 2021 and QDE – 2nd International Conference on Quenching and Distortion Engineering Conference, Berlin
 17. Narayan NM, Moqadam SI, Ellendt N, Fritsching U (2023) Multiphase numerical modeling and investigation of heat transfer for quenching of spherical particles in liquid pool. *Int J Therm Sci* 186(April):2023
 18. Mehdi B, Gopalkrishna SB, Narayan NM, Stephan R, Woche H, Specht E, Fritsching U (2021) Quenching of moving metal plates with flat sprays and single full jet nozzle. In 3. Aachener Ofenbau- und Thermoprozess-Kolloquium, Aachen 323–330 (ISBN: 978-3-96463-021-6)
 19. Wang B, Lin D, Xie Q, Wang Z, Wang G (2016) Heat transfer characteristics during jet impingement on a high-temperature plate surface. *Appl Therm Eng* 100:902–910
 20. Nallathambi A, Specht E (2009) Estimation of heat flux in array of jets quenching using experimental and inverse finite element method. *J Mater Process Technol* 209:5325–5332
 21. Malinowski Z, Hadała B (2018) Implementation of one and three dimensional models for heat transfer coefficient identification over the plate cooled by the circular water jets. *Heat Mass Transf* 54:2195–2213
 22. Orlande H, Özsisik M (2000) *Inverse Heat Transfer: Fundamentals and Applications*. Taylor & Francis
 23. Huang C-H, Wang S-P (1999) A three-dimensional inverse heat conduction problem in estimating surface heat flux by conjugate gradient method. *Int J Heat Mass Transf* 42:3387–3403
 24. Alifanov OM (1998) *Inverse heat transfer problems*. Springer, ISBN 364276438X
 25. Woodbury KA (2003) *Inverse Engineering Handbook*. Crc Press, ISBN 0-8493-0861-5
- Publisher's Note** Springer Nature remains neutral with regard to jurisdictional claims in published maps and institutional affiliations.